ISSN 0023-1584, Kinetics and Catalysis, 2007, Vol. 48, No. 1, pp. 103–115. © MAIK "Nauka/Interperiodica" (Russia), 2007.
Original Russian Text © G.N. Il'inich, A.V. Romanenko, R.I. Kvon, V.B. Fenelonov, V.I. Zaikovskii, A.V. Ishchenko, 2007, published in Kinetika i Kataliz, 2007, Vol. 48, No. 1, pp. 110–122.

Direct Synthesis of Nitrogen-Containing Filamentous Carbon on a High-Percentage Ni–Cu Catalyst

G. N. Il'inich[a], A. V. Romanenko[a], R. I. Kvon[a], V. B. Fenelonov[a], V. I. Zaikovskii[a], and A. V. Ishchenko[b]

[a] *Boreskov Institute of Catalysis, Siberian Branch, Russian Academy of Sciences, pr. Akademika Lavrent'eva 5, Novosibirsk, 630090 Russia*

[b] *Novosibirsk State University, ul. Pirogova 2, Novosibirsk, 630090 Russia*

E-mail: ig@catalysis.nsk.su

Received May 31, 2005

Abstract—Nitrogen-containing catalytic filamentous carbon (N-CFC) of chemical composition NC_{18}–NC_{104} has been synthesized by the decomposition of pyridine (Py) from gaseous mixtures with argon or H_2 at 550–800°C on Ni/Al_2O_3 (Ni) and $Ni–Cu/Al_2O_3$ (Ni–Cu) high-percentage catalysts. The activity of the Ni–Cu catalyst in Py decomposition in mixtures with H_2 is about one order of magnitude higher than its activity in Py/Ar mixtures (more than 70 g N-CFC per metal gram in 4.5 h at 750°C), which is interpreted as arising from the nickel-catalyzed hydrogenation of Py. The formation and growth of carbon fibers occurs through the decomposition of Py (from Ar/Py mixtures) and/or Py hydrodenitrification products (from H_2/Py mixtures). The carbon material has been characterized by elemental analysis, low-temperature nitrogen adsorption, high-resolution transmission electron microscopy (HRTEM), and X-ray photoelectron spectroscopy (XPS). The effect of the noncatalytic reactions of Py and its transformation products on the composition and texture of N-CFC is discussed.

DOI: 10.1134/S0023158407010144

New graphite-like C_xN structures (nitrogen-containing carbon nanotubes and nanofibers) have gained enormous attention during the last decade. The unique electronic, mechanical, and vibrational properties of these materials open up new areas for their application, such as nanotechnologies, materials design for composites and electrochemical and electrophysical sensors, and others [1–4]. Presumably, C_xN nanotubes/nanofibers can behave as metals; they can have high electrical conductivity due to extra electron pairs that conjugate with the delocalized π system of the hexagonal lattice. From the chemical standpoint, the substitution of nitrogen atoms (each having one electron more than a carbon atom) for some carbon atoms may alter the chemical properties of the carbon material; the resulting systems will have a higher reactivity to electron-acceptor molecules. This can extend the application of these materials in adsorption–catalytic processes (the synthesis of functionally active sorbents, supports for catalysts, and metal–carbon catalytic compositions [5–13]).

The catalytic methods for the production of C_xN structures (multiwalled carbon nanotubes and nanofibers) are based on the gas-phase decomposition of nitrogen-containing hydrocarbon precursors in the presence of Group VIII 3*d* metals (Fe, Co, Ni). The following compounds were tested as precursors: heteroatomic hydrocarbons such as pyridine, acetonitrile [14–16], triaminotriazine (melamine) [17–19], aminodichlorotriazine [19, 20], and dimethylformamide [21] mixed with an inert gas, H_2, CH_4, or C_2H_2; nickel phthalocyanine [22, 23]; and mixtures of CO or CH_4 with NH_3 [24, 25] or even with N_2 [26]. Dai et al. [24] described the synthesis of single-walled carbon nanotubes by the decomposition of CO + NH_3 mixtures on molybdenum particles at 1200°C. The amount of nitrogen incorporated into the carbon framework is a function of synthesis parameters, such as the feed composition, catalyst, temperature, and even flow rate. The C_xN structures manufactured by catalytic methods have comparatively low nitrogen concentrations (less than 15 at %; $x \geq 6$) [3, 4]. However, Tang et al. [21] synthesized nanofibers with an extraordinary high nitrogen concentration (20 at %, $x = 5$) by the decomposition of dimethylformamide on a supported FeMo catalyst manufactured by sol–gel technology. The fibers had an unusual pearl-necklace-like morphology. The decomposition of nitrogen-containing hydrocarbons usually produces C_xN structures with higher nitrogen concentrations than in the pyrolysis products of methane mixed with ammonia or N_2. The relevant literature shows that the existing catalytic methods do not ensure sizable yields of nitrogen-containing nanotubes or nanofibers.

In works [14, 15], we described the synthesis of carbon nanofibers through the catalytic decomposition of CH_4 or $CH_4 + H_2$ with addition of nitrogen-containing hydrocarbons, e.g., pyridine or acetonitrile. The cata-

Table 1. Catalyst composition

Catalyst	Composition, wt %	Ni and Cu, wt %	Cu/Ni, at/at
Ni	93 NiO*	Ni(73)	0
Ni–Cu	82 NiO, 5 CuO*	Ni(64.5)–Cu(4.0)	0.06

* Al_2O_3 up to 100%.

lysts used were high-percentage Ni and Ni–Cu catalysts, which are efficient in the synthesis of carbon fibers (catalytic filamentous carbon, CFC) from methane rough materials. The yield of methane CFC on the Ni–Cu catalyst at 650°C was ≥700 g/g Ni [27]. We obtained 40–50 g of N-CFC per metal gram, containing 5 wt % nitrogen, at 750°C on the Ni–Cu catalyst. However, the highest yield was achieved when methane was fully excluded from the reaction gas: 70 ± 5 g N-CFC/g metal was obtained [unpublished data]. The resulting samples also had a more homogeneous morphology. In this context, it is pertinent that our data poorly match the data of Nakajima and Koh [16]: Nakajima and Koh proved the inertness of ultrafine nickel in the synthesis of C_xN nanofibers from pyridine (Py) mixed with H_2. The main distinction between the two approaches is that Nakajima and Koh [16] employed higher decomposition temperatures (800–950°C) than in our synthesis.

An essential weakness of the approach developed was poor precision, associated with the oligomer and resin formation as a result of noncatalytic transformations of Py or its derivatives. Downs and Baker [28], authorities on the synthesis of fibrous carbon on metal catalysts, in the early 1990s stressed the necessity of finding optimal parameters for minimizing these noncatalytic transformations.

Here, we report the detailed investigation of N-CFC synthesis from Py mixed with H_2 or Ar on high-percentage Ni/Al_2O_3 (hereafter, Ni) and $NiCu/Al_2O_3$ (hereafter, NiCu) catalysts. Our task was to elucidate the possible pathways of Py transformations and to find the parameters at which Py pyrolysis is mainly catalytic and occurs at high rates. Low-temperature nitrogen adsorption, high-resolution transmission electron microscopy (HRTEM), and X-ray photoelectron spectroscopy (XPS) were used to characterize the pore structure, morphology of fibrous deposits, the composition of the samples, and the nature of the nitrogen-containing groups; the indicated characteristics were also studied as dependent on the synthesis parameters such as the carrier gas and pyridine concentration in the vapor–gas mixture, pyrolysis temperature, and the contact time between the reaction mixture and catalyst. The results may be of both theoretical and applied significance for the purposed synthesis of C_xN nanotubes/nanofibers with a controlled set of properties for use in the adsorption and catalytic transformations of supports and design of carbon composites and advanced materials for nanotechnologies.

EXPERIMENTAL

Catalytic Experiments

N-CFC samples were prepared by the decomposition of H_2/Py and Ar/Py gaseous mixtures containing 10 or 15 mol % Py at 550–800°C and atmospheric pressure. Hydrogen (>99.99%) and argon (>99.99%) were used as received. Reagent-grade pyridine was predried over KOH.

The reaction was accomplished in a vertical flow-through reactor with a vibrofluidized bed of the Ni or Ni–Cu catalyst (0.25–0.50 mm fraction). Catalyst samples were prepared following the procedures described in works [29, 30]. Their compositions are listed in Table 1. The catalyst sample weight was 0.05 g unless specified otherwise. The catalysts were reduced in situ in flowing hydrogen at 550°C for 2 h. Then, the reactor was brought to the required temperature, the hydrogen feeding was stopped, and the vapor–gas mixture of the set composition was fed at 1–7 l/h. The vapor–gas mixture was prepared by bubbling the dry reaction gas through an evaporator filled with Py, which was mounted upstream of the reactor. The Py concentration in the mixture was controlled through the evaporator temperature. The reaction loop was enclosed into a thermal cabinet maintained at 120–125°C in order to keep the Py vapor from condensing. The reaction mixture leaving the reactor entered a water trap in which the reaction byproducts and Py vapor were entrapped. The pyrolysis duration was 2.3 or 4.5 h. Before being discharged, N-CFC granules were cooled with flowing argon to room temperature.

Physicochemical Characterization of N-CFC

The carbon material was characterized using a combination of chemical analysis, low-temperature N_2 adsorption, HRTEM, and XPS spectroscopy.

Low-temperature N_2 adsorption. The adsorption measurements were carried out at 77 K on a Micromeritics ASAP 2400 instrument. Carbon samples were first trained at 573 K to a residual pressure of 10^{-3} Torr. The specific surface area S_{BET} was calculated from the initial portion of the adsorption isotherm with P/P_0 = 0.05–0.20. The total pore volume V_Σ with effective pore diameters up to 100 nm was calculated from the N_2 uptake for P/P_0 = 0.98. The micropore volume V_μ, accessible to nitrogen, was estimated by a comparison method developed in [31], which is in many respects an analogue of the α_s technique proposed by Sing [32]. The average pore size D_{pore} was calculated from $D_{pore} = 4V_{pore}/S_{BET}$.

HRTEM. A JEM-2010 high-resolution electron microscope was used with an accelerating voltage of 200 kV (the lattice resolution was 1.4 Å). The samples

Table 2. Parameters of Py decomposition from mixtures with H_2 and Ar and the major products

N-CFC sample	N-CFC synthesis parameters			N-KBУ		Oligomers
	mixture	T, °C	τ, s	Y, g C/g M	N, wt %	
Ni–Cu catalyst						
N-301[1]	H_2 + 10% Py	550	0.03	33	1.0	–
N-159[2]			0.06	22	1.0	–
N-319[1, 2]		650	0.03	30	1.2	–
N-241			0.06	42	2.0	–
N-293			0.06	40	1.4	–
N-270			0.11	37	1.7	–
N-219			0.17	37	2.3	–
N-317[2]		700	0.03	50	1.8	–
N-286[2]		750	0.025	40	3.4	–
N-285			0.03	70	2.9	+[3]
N-305			0.03	73	2.7	+[3]
N-233			0.17	30	2.8	++[3]
N-288[1, 2]		800	0.03	26	3.2	++[3,4]
N-273	H_2 + 15% Py	550	0.06	40	2.2	–
N-277		650	0.06	28	2.6	+[3]
N-256		750	0.03	18	3.0	++[3]
N-318	Ar + 10% Py	750	0.06	5	5.2	–
N-205	Ar + 15% Py	550	0.11	3	3.0	–
N-207		750	0.11	6	5.0	–
Ni catalyst						
N-302[1]	H_2 + 10% Py	550	0.03	34	0.7	–
N-173		750	0.03	15	2.2	++[3]

[1] 0.025 g catalyst.
[2] Reaction time: 2.3 h.
[3] Colored, water-soluble liquid of an unidentified composition.
[4] Trace resin at the reactor outlet.

were prepared by ultrasonic dispersion in ethanol followed by spreading of the suspension over the standard grid of the sample holder.

X-ray photoelectron spectroscopy. The XPS experiments were carried out on a VG ESCALAB HP photoelectron spectrometer using MgK_α and AlK_α radiation with the 2×10^{-8} mbar pressure of background gases in the working chamber. The spectrometer was calibrated against the lines Au $4f_{7/2}$ (84.0 eV) and Cu $2p_{3/2}$ (932.7 eV). Correction for charging was applied using an internal standard (the carbon peak at E_b = 284.4 eV). The test pellets were ground, then indented into a double-sided sticky band mounted on the sample holder. The composite spectra were decomposed into individual peaks, and the parameters of the components were determined using XPS Peak software [33, 34].

RESULTS AND DISCUSSION

Catalytic Reactions of Gaseous Py Mixed with H_2 or Ar

To determine the parameters that would direct Py decomposition along the catalytic route, we studied how the synthesis temperature, feed composition, decomposition duration, and contact time τ (τ = V/v, s, where V is the catalyst volume and v is the volume rate

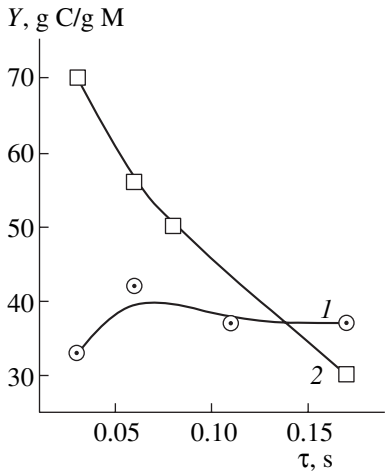

Fig. 1. N-CFC yield vs. contact time between the reaction mixture and the catalyst at (*1*) 650 and (*2*) 750°C on the Ni–Cu catalyst. H_2/10% Py. Pyrolysis duration: 4.5 h.

of the reagents under the STP) affect the product composition, N-CFC yield (*Y*), and the texture parameters of the samples.

The data complied in Table 2 show us the general trends in the variation of the product composition as a function of synthesis parameters for Py decomposition from mixtures with Ar or H_2. The activities of the Ni and Ni–Cu catalysts in the low-temperature (550°C) pyrolysis of H_2/Py mixtures are roughly identical. At 750°C, the use of the Ni–Cu catalyst increases the N-CFC yield about fivefold. The role of copper in the hydrocarbon decomposition catalyzed with Group VIII transition metals (nickel, iron) is extensively discussed in the literature (see, e.g., Fenelonov's monograph [35] and references cited therein). However, the issue is beyond the scope of this work.

From Table 2, it follows that byproducts (low-molecular-weight oligomers) appeared in the final mixture after H_2/Py decomposition at quite low temperatures (650°C). Their formation rate increased with temperature elevation. There is an inverse proportion between the catalyst activity in CFC formation and the amount of the oligomers produced. Gas chromatography showed NH_3 in the final gas mixture in all experiments.

Figure 1 displays the carbon yield from H_2/10%Py decomposition versus contact time τ. The maximal N-CFC yield (70 g C/g M) was observed at 750°C at low τ (~0.03 s). The increasing contact time and the decreasing flow rate of the reagents (from 6 to 1 l/h for samples N-285 and N-233, respectively; Table 2) displaced the equilibrium between the catalytic decomposition of Py and the high-temperature (noncatalytic) oligomerization of Py and/or its transformation products toward the latter. The oligomer proportion in the products increased, while the yield of N-CFC decreased. At low temperatures (550 and 650°C), the N-CFC yield was 30–40 g carbon per metal gram without any prominent correlation between the yield and contact time.

The activity of the Ni–Cu catalyst in N-CFC synthesis from H_2/10%Py was appraised for the region of low τ (0.03 s), at which the effect of the side reactions on N-CFC formation at temperatures below 750°C can be ignored, although with some assumptions. The relevant curves (Fig. 2a; curves *1*, *2*, respectively) are different for the samples prepared by decomposition for 4.5 and 2.3 h. Curve *2* has a rise at relatively low temperatures and a maximum at about ~700°C. The samples synthesized at temperatures in this range had similar specific surface areas (~300 m^2/g). Above 700°C, the carbon yield decreased but the oligomer concentration in the products increased dramatically (Table 2). The specific surface area became one order of magnitude lower: 284 and 28 m^2/g for the samples synthesized at 700 and 800°C, respectively (Fig. 2b, curve *2*). We tend to explain these experimental results by the fact that starting at ≥650°C, the oligomers were pyrolyzed on the

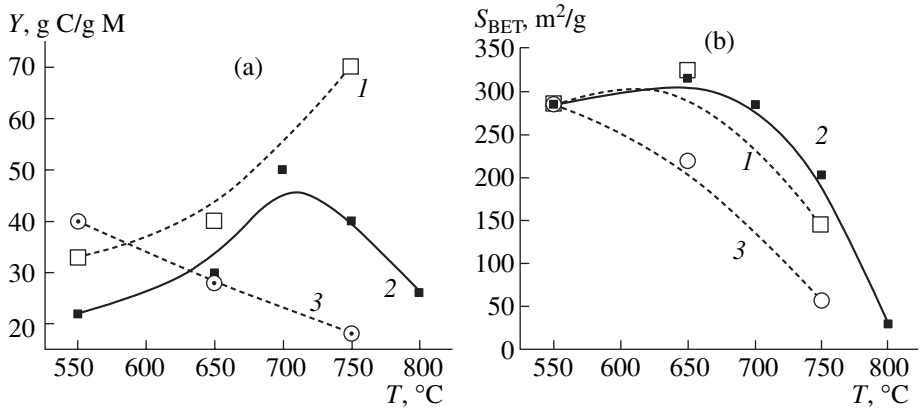

Fig. 2. Panel (a): N-CFC yield vs. reaction temperature for N-CFC samples prepared by H_2/Py pyrolysis on the Ni–Cu catalyst. Panel (b): the specific surface area vs. reaction temperature for the same samples. Contact time: 0.03 s. (*1*) H_2/10%Py, 4.5 h; (*2*) H_2/10% Py, 2.3 h; and (*3*) H_2/15% Py, 4.5 h.

Table 3. Noncatalytic transformations of Py

T, °C	Py/H_2[1]	Py/Ar[1]
550	No products	No products
750	Trace soot or very small pellets Small amounts of unidentified hydrocarbons and oligomers	The reactor outlet is coated with a film of partially pyrolyzed resin Small amounts of unidentified hydrocarbons
800[2]	–	No amorphous carbon [16]
1000[2]	–	Amorphous carbon of composition $NC_{14}H_{0.6}$ [16]

[1] 15 mol % Py; flow rate, $v = 3$ l/h; supply duration, 4.5 h.
[2] 0.02 atm Py with a total pressure of 1 atm; $v = 3$ l/h; supply duration, half-day.

nascent nanofibers. The disordered carbon produced by the decomposition, first, deactivated the catalyst through blocking the surface of active catalytic particles; second, it accumulated in the structure of growing carbon fibers, affecting the texture parameters of the carbon deposits. Evidently, these speculations can likewise explain the temperature variation of the carbon yield in the set of runs that lasted 4.5 h. The monotonic increase in the carbon yield with temperature until 750°C in this set of runs (curve *1* as opposed to curve *2*) is only due to the greater portion of noncatalytic carbon in the deposits obtained in the longer experiments. The N-CFC amounts obtained from Py/H_2 pyrolysis at 800°C after 4.5 h are not displayed on curve *1*: the carbon deposits obtained in the experiments that lasted longer than 2.3 h were caked agglomerates of carbon pellets and pyrolyzed resin. The product was compositionally and structurally heterogeneous. For comparison, curves *3* on Figs. 2a and 2b show the carbon yield and specific surface area versus temperature for H_2/15% Py pyrolysis for 4.5 h. Noticeable amounts of oligomers were observed even at 650°C (Table 2). For the Py-rich mixtures, both the N-CFC yield and the specific surface area decreased monotonically as the temperature rose.

When hydrogen was replaced by an inert gas (Ar or N_2), the carbon yield dropped by about one order of magnitude at all temperatures (550, 650, and 750°C). For Ar/Py decomposition at 750°C on the Ni–Cu catalyst for 4.5 h, the yield was about 5–6 g C/g M (Table 2). Oligomer formation was not observed. Following Nakajima and Koh [16], a higher temperature range is optimal for preparing filamentous carbon compounds NC_x from Py mixed with Ar on finely dispersed nickel. At 850–950°C (0.02 atm Py with a total pressure of 1 atm), Nakajima and Koh [16] obtained 8–10 g of filamentous carbon of composition NC_x ($x = 25$–36) per metal gram; the product was free of amorphous carbon.

Pyridine Transformations in the Absence of Catalysts

We carried out a special set of experiments to appraise the contribution of the noncatalytic transformations of Py into the decomposition of Py/H_2 and Py/Ar. These experiments completely reproduced the catalytic experiments but without catalysts. Moreover, we used new reactors for the blanks in order to avoid the possibility of the occurrence of trace metal on the inner surfaces of the reactor. We chose the parameters of the experiment (Py-rich mixtures, low feed flow rates) that always ensured oligomer formation during the catalytic decomposition of Py/H_2 mixtures.

The blanks showed the absence of any products of noncatalytic reactions at 550°C. The thermal transformations of Py were rather slow even at 750°C regardless of the carrier gas (H_2 or Ar). The composition of the Py-containing mixtures entering the reactor and that of those leaving the reactor were practically the same as analyzed by gas chromatography. The production of a small amount of resin (Table 3) in the experiment with a Py/Ar mixture can be due to the dehydrooligomerization capacity of Py. Noticeable pyrolysis rates are observed at far higher temperatures (1000°C) [16].

Having compared these results with the catalytic data, we inferred that the products of heterocycle splitting, probably unsaturated C_5, or other light hydrocarbons produced by Py hydrogenation on a Ni catalyst are responsible for the oligomerization side processes during the catalytic decomposition of Py/H_2 mixtures.

Pore Structure of N-CFC Samples

Low-temperature nitrogen adsorption was used to study how the synthesis parameters affect the pore structure parameters of N-CFC samples manufactured from H_2/Py mixtures.

Representative adsorption isotherms are displayed in Fig. 3. According to the IUPAC classification (which classifies the typical shapes of capillary-adsorption hysteresis loops), the isotherms for all samples can be classified as intermediate between type H1 and type H3 [32]. Loop H1 is characteristic of monodisperse and fairly homogeneous packed porous bodies. Loop H3 is characteristic of porous systems with mainly slit-shaped pores. All isotherms have a hysteresis loop in the range of $0.45 \le P/P_0 < 1$, indicating the presence of

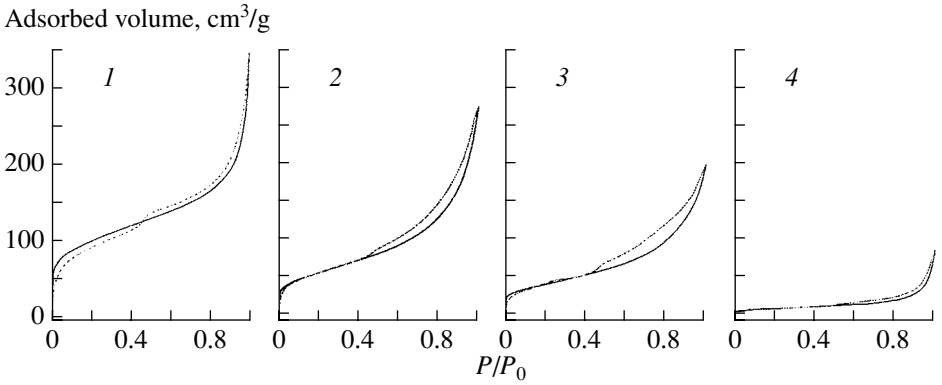

Fig. 3. Low-temperature N_2 adsorption isotherms for N-CFC samples prepared by H_2/10% Py decomposition: (*1*) 650°C, $Y \sim$ 40 g C/g M; (*2*) 750°C, $Y \sim 40$ g C/g M; (*3*) 750°C, $Y \sim 73$ g C/g M; and (*4*) 800°C, $Y = 26$ g C/g M.

mesopores with sizes up to 100 nm, and a rise at $P/P_0 \longrightarrow 1$, which is associated with larger pores.

The pore-structure parameters for some N-CFC samples are compiled in Table 4. Clearly, the texture parameters can be widely varied with the use of the synthesis method in question. The specific surface areas ranged from ~30 to ~360 m^2/g. The pore volumes V_Σ were 0.17–0.54 cm^3/g with the average pore diameter D_{pore} ranging from 5 to ~20 nm. The samples produced at 550 and 650°C had close S_{BET} values (325 ± 35 m^2/g) with roughly equal carbon proportions (~40 g C/g M). The micropore volumes calculated from the adsorption isotherms, V_μ, were 0.02–0.04 cm^3/m or 6–7% of the total pore volume. The samples produced at 750 and 800°C lacked micropores. The S_{BET} versus synthesis temperature curve (Fig. 2b, curve *2*) has an inflection at about 650°C. The S_{BET} values for the samples prepared at 650 and 800°C differed by more than one order of magnitude. In the samples prepared from mixtures with a higher (15%) Py concentration, S_{BET} decreased mono-

Table 4. Pore-structure parameters for N-CFC prepared from H_2/Py mixtures

N-CFC sample	T_{sint}, °C	[Py], mol %	Pore-structure parameters			
			S_{BET}, m^2/g	V_Σ, cm^3/g	V_μ, cm^3/g	D_{pore}, nm
Ni–Cu catalyst						
N-301	550	10	282	0.376	0.024	5
N-273		15	285	0.340	0.020	5
N-319	650	10	313	0.424	0.008	5
N-241		10	359	0.537	0.037	6
N-219		10	295	0.423	0.024	6
N-277		15	219	0.328	0.008	6
N-317	700	10	284	0.359	0.001	5
N-286	750	10	201	0.391	0.001	8
N-285		10	144	0.309	0	9
N-305		10	104	0.285	0	12
N-233		10	32	0.169	0.003	21
N-256		15	56	0.172	0	12
N-288	800	10	28	0.131	0	18
Ni catalyst						
N-302	550	10	267	0.334	0.024	5
N-173	750	10	47	0.130	0	11

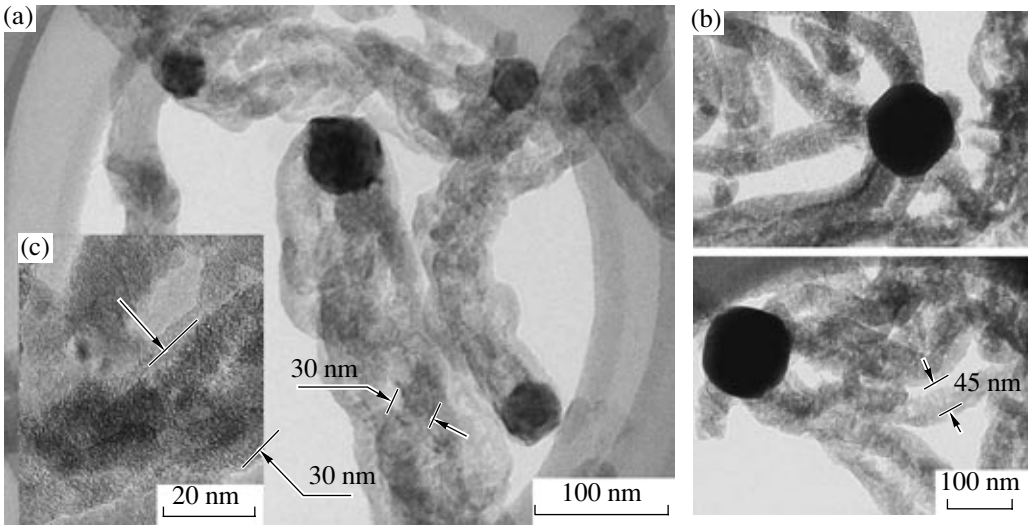

Fig. 4. Panels (a, b): the representative morphology of N-CFC grown on the Ni–Cu catalyst from H_2/10% Py at (a) 550 and (b) 650°C. Panel (c): the structure of thin filaments prepared at 550°C.

tonically as temperature rose to 750°C (Fig. 2b, curve *3*).

The above data can be explained by the fact that oligomers, which are by-products of the process, start to pyrolyze at quite a low temperature (≤650°C) on the surface of carbon fibers and accumulate in the carbon matrix in amounts that alter the pore-structure parameters. Comparing the adsorption isotherms, one can see that the finest pores are the first to fill; then, mesopores are filled.

HRTEM Study

Electron microscopy data show various morphologic types of carbon fibers formed from Ar/Py and H_2/Py mixtures. Most fibers prepared from Py/H_2 at 550 and 650°C have octopus morphology: several thin nanofibers with diameters of about 15–30 nm spring out of a faced particle of a NiCu alloy (Fig. 4). Some carbon layers are oriented approximately normal to the fiber axis (Fig. 4c). A loose, disordered structure is characteristic of the fibers. This structure dictates the texture parameters of the samples, namely high specific surface areas and porosities (Fig. 2b, Table 4). Being chaotically entangled during growth, several thin fibers form bundles of thicker fibers. Most secondary fibers have diameters of 50–100 nm (Fig. 4a). Similar morphologies were observed upon the pyrolysis of methane on NiCu alloy catalysts [36, 37] and NiCu/Al_2O_3 high-percentage catalysts [38, 39] at temperatures up to 1000 K. According to the carbide cycle mechanism developed by Buyanov [40], gaseous hydrocarbons are decomposed on one face of a catalytically active particle to yield carbide-like M_xC_y intermediates; the latter diffuse into the bulk of the particle and decompose on other faces, yielding carbon. The appearance of octopus morphology is assigned to the reconstruction of catalyst particles under the reaction conditions. As a result of segregation and faceting in the NiCu alloy, the catalyst surface is fragmented into alternating portions of Ni(110) and (100) faces, at which hydrocarbons are pyrolyzed, and (111) and (311) faces, at which carbon is separated and crystallizes into graphite [41]. In addition, the structure and properties of the active sites of the catalyst, determining the morphology of the filaments, can be modified in the reaction with the gas components, e.g., sulfur compounds [41, 42] and H_2 [43]. Mishakov et al. [44] observed octopus formation in the decomposition of $C_2H_4Cl_2$ in a mixture with H_2 at 650°C on the Ni/Al_2O_3 high-percentage catalyst without copper added.

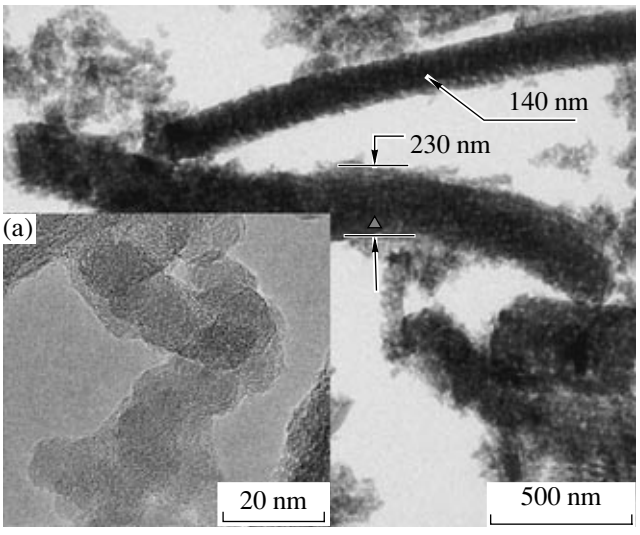

Fig. 5. Micrograph of an N-CFC sample prepared by H_2/10% Py pyrolysis at 750°C. a—Admixture of twisted graphite filaments, characteristic of Py decomposition in argon.

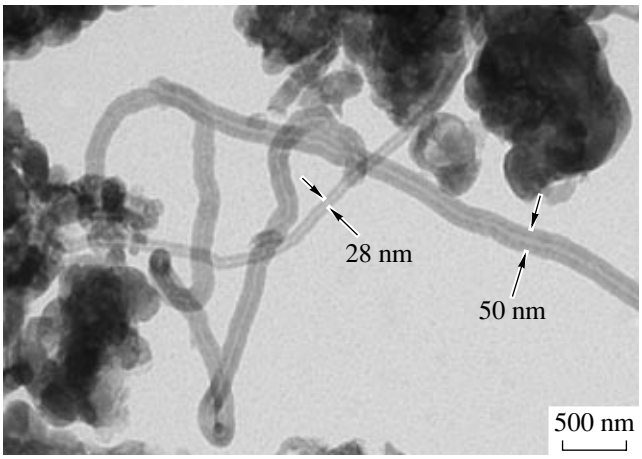

Fig. 6. Micrograph of an N-CFC sample prepared by Ar/Py decomposition at 750°C.

At a high temperature (750°C) of H_2/Py pyrolysis, the fiber diameters ranged from 15 to 300 nm (Fig. 5). The morphologies characteristic of the decomposition of Py from mixtures with an inert gas (see below) were observed in small amounts. These were thin graphite nanofibers and carbon nanotubes. A minor amount of pyrocarbon was also observed. These observations match the catalytic experiments, in which significant amounts of oligomers were formed upon the high-temperature decomposition of H_2/Py mixtures (Table 2), and the above-described pore structures of the samples.

A fundamentally different microstructure was observed for the N-CFC samples prepared from Ar/Py mixtures under the same conditions (Fig. 6). These samples were compositionally heterogeneous. Carbon existed in them in several forms. Rounded particles were dominant; at high resolution, they looked like bands and coils of thin, tightly twisted graphite nanofibers with sizes of 10–30 nm (Fig. 7). One can see on the straight portions of fibers that graphite layers lie normal to the fiber axis in the central part of the fiber, yielding to the fiber surface at an angle (Fig. 7a).

There were small amounts of thin fibers with a hollow channel, compartmented with partitions of several carbon layers, and fibers with the morphology intrinsic in the N-CFC samples grown from H_2/Py (which is quite understandable, because some amount of H_2 is liberated upon Py decomposition).

Chemical Composition of N-CFC

The chemical compositions of N-CFC samples calculated from the chemical analysis data, NC_xH_y, are listed in Table 5. The C/N ratio (at/at) in these samples ranged from 18 to 104; this quantity was strongly affected by many factors: the nature of the catalyst, the composition of the reaction mixture (hydrogen or an inert carrier gas, Py concentration), and the synthesis temperature. The synthesis parameters being identical,

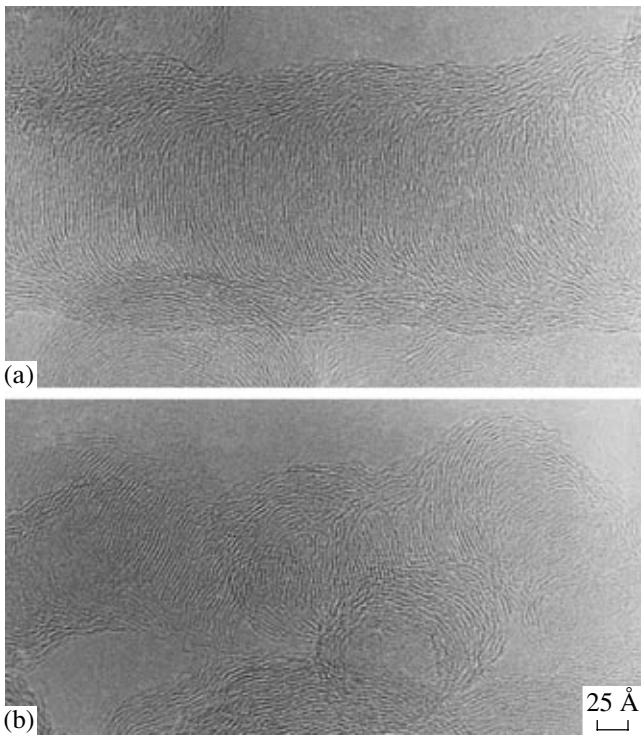

Fig. 7. HRTEM micrographs of carbon filaments in the structure of N-CFC prepared from Ar/Py at 750°C.

the C/N ratio was lower in the samples prepared by Py pyrolysis from the mixtures with an inert gas. N-CFC samples of composition $NC_{18}H_{1.4}$ were prepared by the pyrolysis of a Py/Ar mixture on the Ni–Cu catalyst at 750°C. The samples contained two times more nitrogen atoms than the samples prepared from the Py/H_2 mixture whose chemical composition was determined as $NC_{32–38}H_{1.6–3.2}$. The C/H (at/at) ratio calculated from this composition increases as the temperature rises from 550°C (C/H = 8–9) to 800°C (C/H = 47). This trend can be due to the decreasing number of carbon atoms in an aliphatic environment, the increasing aromaticity of the hydrocarbons, and the structural alterations of the nitrogen-containing groups.

The surface composition of N-CFC samples was studied by means of XPS; this method determines the concentrations of chemical elements in surface layers with thicknesses to 10 nm (Table 5). The survey spectra showed Ni, C, N, and O on the surface of all N-CFC samples (Fig. 8). Because the synthesis parameters excluded the contact of the reagents and nascent carbon deposit with oxygen, the oxygen-containing groups likely originated from the oxygen and water vapor adsorbed by the sample from air during storage. The existence of large amounts of adsorbed oxygen on porous carbon materials is a well-known fact.

The bulk composition of samples usually differs from the surface layer composition. There is one more fundamental difference between the samples prepared

Table 5. Chemical composition of N-CFC samples[1] prepared by various decomposition schedules

N-CFC sample	T, °C	Reaction mixture[2]	N-CFC yield, g C/(Ni + Cu) g	Composition		State of surface N atoms, %		
				NC_xH_y (bulk)[3]	NC_x (surface)[4]	N_{Py}	N_{Pyr}	N_Q
N-301	550	H_2 + 10% Py	33	$NC_{104}H_{13}$	–	–	–	–
N-273		H_2 + 15% Py	40	$NC_{50}H_{7.1}$	NC_{60}	40	54	6
N-293	650	H_2 + 10% Py	46	–	NC_{85}	34	58	8
N-277		H_2 + 15% Py	28	$NC_{39}H_{4.3}$	NC_{55}	36	51	13
N-286	750	H_2 + 10% Py[5]	40	$NC_{32}H_{3.2}$	NC_{31}	44	41	15
N-285		H_2 + 10% Py	70	$NC_{38}H_{2.7}$	NC_{46}	42	38	20
N-256		H_2 + 15% Py	18	$NC_{36}H_{1.6}$	NC_{43}	37	48	15
N-288	800	H_2 + 10% Py	26	$NC_{33}H_{0.7}$	NC_{21}	27	46	27
N-205	550	Ar + 15% Py	~3	$NC_{27}H_{1.4}$	NC_{15}	29	58	13
N-206	650	Ar + 15% Py	3	$NC_{25}H_2$	NC_{11}	30	52	18
N-207	750	Ar + 15% Py	5	$NC_{18}H_{1.4}$	NC_{10}	42	41	17

[1] Apart from the catalyst components.
[2] Decomposition time: 4.5 h.
[3] From elemental analysis data.
[4] From XPS data.
[5] Decomposition time: 2.3 h.

from H_2/Py and Ar/Py mixtures. In the samples from Ar/Py mixtures, the surface nitrogen concentration was higher than the bulk concentration. For the samples prepared from H_2/Py mixtures at 550–750°C, on the contrary, the nitrogen concentrations in the surface layer were usually lower than in the bulk (Table 5). A likely explanation must include both the features of Py decomposition and carbon fiber formation from mixtures with different carrier gases (they will be discussed below) and the possible routes of nitrogen incorporation into carbon structures (they are to be studied).

Nitrogen exists on the N-CFC surface in three chemical states with binding energies E_b of 398.6, 401.0, and 402.3 eV. The intensity ratio for these states is a function of the synthesis temperature, batch composition, and decomposition duration (Table 5). Figure 9 displays the decomposition of the N 1*s* spectrum to individual peaks for a sample synthesized from H_2/Py at 800°C.

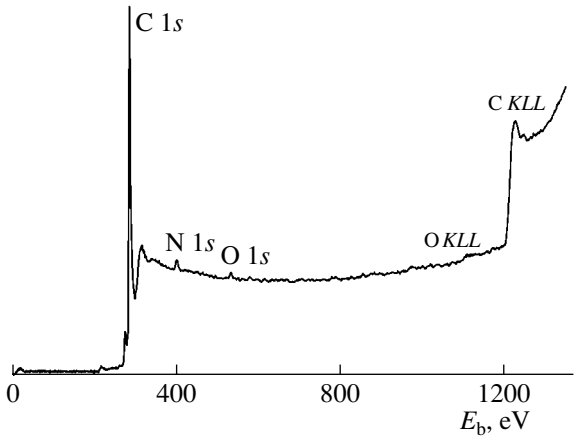

Fig. 8. Scan XPS spectra of samples prepared from H_2/10% Py at 750°C.

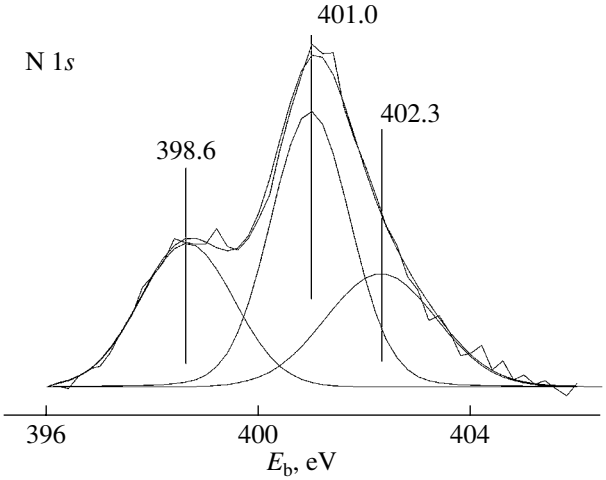

Fig. 9. N 1*s* spectrum of a sample prepared from H_2/10% Py at 800°C.

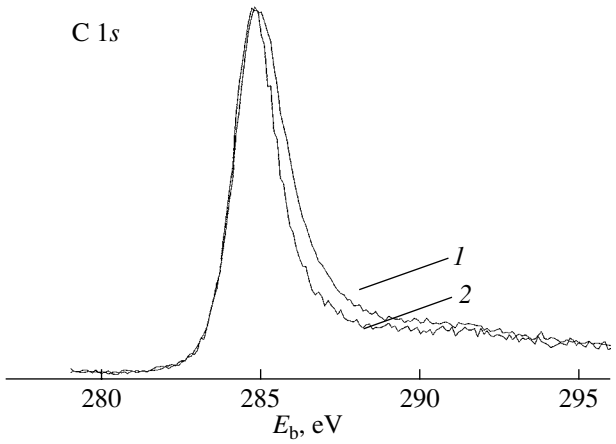

Fig. 10. C 1*s* spectra of samples prepared from H_2/10% Py at (*1*) 800°C and (*2*) 650°C.

The N1*s* state, with the lowest binding energy (E_b = 398.6 + 0.2 eV), is firmly assigned to nitrogen atoms in pyridine-type structures (N_{Py}) located at the fringes and defects of carbon layers. More data is needed to identify the other two nitrogen species. According to [45, 46], the peak at E_b ~ 401 eV is due to pyrrole-type nitrogen N_{Pyr}. The value of E_b ~ 401 eV is also assigned to amino nitrogen atoms [47, 48]. The direct transformation of nitrogen-containing structures upon the carbonization of some model hydrocarbons was studied in [46, 49]. The model hydrocarbons used were polyvinylpyridine, dibenzopyrrole [46], and N-substituted anthracenes bearing nitrogen atoms in various positions: acridine, 9-aminoacridine, 9-cyanoanthracene, and 2-aminoanthracene [49]. It was found that cyano groups and especially amino groups have a low thermal stability [49]: they disappear even at about 500°C, partially converting to the more stable pyridine- and pyrrole-like structures. The aromatic nitrogen is the most difficult to eliminate. Most likely, the surface state with E_b ~ 401 eV in N-CFC samples refers to pyrrole-type nitrogen atoms (N_{Pyr}), probably, with some contribution from the amino and cyano nitrogen atoms at low synthesis temperatures (550°C). The third state of the nitrogen is assigned by some researchers to the nitrogen linked to carbon atoms in graphene layers [3–6], so-called tertiary or quaternary nitrogen (N_Q). The state with E_b ~ 402.1–402.3 eV exists in all samples synthesized from Py/Ar at 550–750°C (Table 5). However, the intensity of this peak (if it occurs at all) is low in the N-CFC samples synthesized from Py/H_2 at 550°C and increases with increasing decomposition temperature.

The C 1*s* spectra carry information about the state of surface carbon atoms (Fig. 10). In the low-temperature samples prepared from H_2/Py at 550 and 650°C, the structure of the C 1*s* lines corresponds to the graphite carbon (E_b = 284.4 eV; peak half-width, 1.3 eV). We think that the broadening of the C 1*s* peak in the sample prepared at 800°C can be due to nongraphite carbon: there were large amounts of the products of resin pyrolysis in the sample, which matches the adsorption data. The specific surface areas in samples N-295 and N-288 differ by one order of magnitude (325 against 28 m^2/g); not only does sample N-288 lack micropores, but there are almost no mesopores in this sample (Fig. 3; curves *1*, *4*). Likely, the highest surface concentration of tertiary nitrogen atoms (the N 1*s* state with E_b ~ 402.1 eV) is partially due the moiety of nitrogen-bearing fragments in pyrolytic carbon.

Competing Pyridine Transformation Reactions in the Supported Nickel Catalyst–Py/H_2 (Ar) System

Catalytic reactions of Py. Much attention is paid to Py hydrodenitrification (HDN) on supported NiMo [50, 51] and CoMo catalysts [52, 53]; this reaction is of practical significance for oil refining. It is known that the reaction is the succession of the following stages: the hydrogenation of Py to piperidine (Pip), hydrogenation of Pip with heterocycle opening, aminopentane (MPA) formation, and MPA splitting to C_5 hydrocarbons; many other compounds can also form as a result of the reactions of the HDN products of Py. Some of them are shown in the scheme.

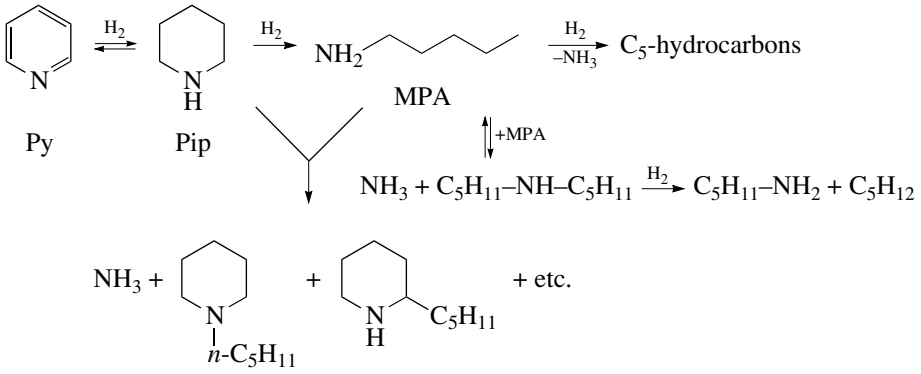

Scheme.

The rate-controlling stage of the HDN is heterocycle opening. Nickel promotes both the hydrogenation of Py and the break of the C–N bond of Pip.

All experimental results discussed above prove that the high activity of Ni(Cu) catalysts in the synthesis of fibrous C_xN compounds is due to the use of Py mixed with H_2 in the range of 550–750°C. Hydrogen is both the carrier gas and the reagent, and the nickel-catalyzed Py hydrogenation with heterocycle opening is, most likely, the main pathway of Py transformation. Carbon filaments are formed by the decomposition of HDN products on the active sites of the catalyst. In a hydrogen-deficient atmosphere, another parallel route is possible, namely, the catalytic decomposition of Py itself to carbon. In the absence of hydrogen (in Py/inert gas mixtures), this is the major route of Py decomposition. The N-CFC formation rates in this route at 550–750°C are not high.

According to the carbide cycle mechanism advanced by Buyanov and colleagues [40], the catalytic decomposition of gaseous hydrocarbons on metals involves the formation of intermediate carbide-like compounds M_xC_y, which subsequently decompose with carbon evolution. The presence of a nitrogen atom in the hydrocarbon molecule is not essential for the mechanism of the process. In view of this, the formation of carbon by the catalytic decomposition of Py is thermodynamically less favorable: the rupture of the strong sp^2 hybrid bonds (with $E_b \sim 680$ kJ/mol) in a Py molecule is required for intermediate carbide-like compounds N_xC_y to form, and high temperatures and low H_2 partial pressures are required in order for N-CFC synthesis to be directed mainly along the second route. The dissociation of a Py molecule adsorbed on the catalyst surface can be the rate-controlling stage of the process.

The existence of at least two possible routes for catalytic Py transformations, whose relative rates are functions of the nature of the carrier gas and temperature, is responsible for the different fiber morphologies and compositions of N-CFC. Recall that the N-CFC samples prepared from H_2/Py mixtures contain only one-half the nitrogen atoms contained in the samples prepared from mixtures with argon. One likely reason is the production of ammonia by the HDN of pyridine and its removal from the reaction mixture together with the gaseous reaction products.

High-temperature Py decomposition and the products of its transformations. In the section concerning noncatalytic Py transformations, we showed that at $T \le 750$°C in the absence of hydrogen, only minor amounts of resins are formed. We think that the products of pyridine HDN are the major source of oligomers in N-CFC synthesis from H_2/Py mixtures. Above 650°C, the oligomers are pyrolyzed on the surface of nascent nanofibers to yield disordered carbon deposits.

From the close values of the pore-structure parameters in the N-CFC samples synthesized from H_2/10% Py mixtures at 550 and 650°C (Table 4), HRTEM data, and XPS data (Fig. 10), we infer that pyrolytic carbon does not play an important role in the formation of the pore structure in this temperature range. Pyridine transformations mainly follow the catalytic route and yield filamentous carbon as the final product. The pore structure of the N-CFC samples manufactured at temperatures above 650°C changes (micropores disappear, V_Σ and S_{BET} decreases), likely due to the change in fiber morphology and (mainly) the increase in the rates of the noncatalytic reactions of oligomerization and oligomer pyrolysis on the fiber surfaces. The different pore structures in N-286 and N-285 samples (Table 4), which were synthesized at similar parameters (750°C; τ = 0.025 and 0.03 s, respectively) but with different durations of Py/H_2 decomposition and different N-CFC yields (40 and 70 g C/g M in 2.3 and 4.5 h, respectively), can be due to both the higher amount of accumulated pyrocarbon and the higher fiber packing density in sample N-285.

Pyrolytic carbon, on one hand, changes the pore structure of N-CFC; on the other, it can block the active sites of the catalyst at which nanofibers are formed and grown, thus deactivating the catalyst. The accumulation of large amounts of pyrocarbon is likely one reason for the dramatic decrease in the N-CFC yield above 700°C (Fig. 2a). The noncatalytic oligomerization and oligomer pyrolysis on the surface of carbon fibers have a stronger affect on the pore-structure parameters of N-CFC and the deactivation of the catalyst when mixtures with higher Py concentrations (H_2/15% Py) are pyrolyzed; the effect is noticeable even at 650°C (Fig. 2a; Tables 2, 4).

To summarize, the low-temperature (550–650°C) decomposition of Py/H_2 mixtures containing no more than 10% Py can ensure N-CFC synthesis under the conditions where Py decomposes mainly catalytically. The resulting N-CFC samples will have fairly high specific surface areas (300–350 m^2/g) and low nitrogen concentrations (≤2 wt %). The decomposition of Py-containing blends at temperatures above 650°C likely cannot fully avoid the effect of the noncatalytic transformations of Py on the activity of the catalyst and the composition and pore structure of N-CFC. However, the set of parameters can be determined to weaken this effect: above all, it is pertinent to use low-Py feeds (containing less than 10 mol % Py) and high volumetric reactant feed rates.

ACKNOWLEDGMENTS

The authors acknowledge the essential contribution of the corresponding member of the RAS V.A. Likholobov to the development of the concept of the work.

REFERENCES

1. Zhou Gang and Duan Wenhui, *J. Nanosci. Nanotechnol.*, 2005, vol. 5, no. 9, p. 1421.
2. Ewels, C.P. and Glerup, M., *J. Nanosci. Nanotechnol.*, 2005, vol. 5, no. 9, p. 1345.
3. Terrones, M., Jorio, A., Endo, M., Rao, A.M., Kim, Y.A., Hayashi, T., Terrones, H., Charlier, J.-C., Dresselhaus, G., and Dresselhaus, M.S., *Mater. Today*, 2004, vol. 7, no. 10, p. 30.
4. Terrones, M., Ajayan, P.M., Banhart, F., Blase, X., Carroll, D.L., Charlier, J.C., Czerw, R., Foley, B., Grobert, N., Kamalakaran, R., Kohler-Redlich, P., Ruhle, M., Seeger, T., and Terrones, H., *Appl. Phys. A: Mater. Sci. Process.*, 2002, vol. 74, no. 3, p. 355.
5. Mangun, Ch.L., Benak, K.R., Economy, J., and Foster, K.L., *Carbon*, 2001, vol. 39, no. 12, p. 1809.
6. Mangun, Ch.L., DeBarr, J.A., and Economy, J., *Carbon*, 2001, vol. 39, no. 11, p. 1689.
7. Yang, Ch.-M. and Kaneko, K., *Carbon*, 2001, vol. 39, no. 7, p. 1075.
8. Yang, Ch.M. and Kaneko, K., *J. Colloid Interface Sci.*, 2002, vol. 255, no. 2, p. 236.
9. Koh, M. and Nakajima, T., *Carbon*, 2000, vol. 38, no. 14, p. 1947.
10. Raymundo-Pinero, E., Cazorla-Amoros, D., and Linares-Solano, A., *Carbon*, 2003, vol. 41, no. 10, p. 1925.
11. Davini, P., *Carbon*, 2003, vol. 41, no. 2, p. 277.
12. Muniz, J., Marban, G., and Fuertes, A.B., *Appl. Catal., B*, 2000, vol. 27, no. 1, p. 27.
13. US Patent 5173466.
14. RF Patent 2147925.
15. Kvon, R.I., Il'inich, G.N., Chuvilin, A.L., and Likholobov, V.A., *J. Mol. Catal. A: Chem.*, 2000, vol. 158, no. 1, p. 413.
16. Nakajima, T. and Koh, M., *Carbon*, 1997, vol. 35, no. 2, p. 203.
17. Terrones, M., Redlich, Ph., Grobert, N., Trasobares, S., Hsu, W.K., Terrones, H., Zhu, Y.Q., Hare, J.P., Cheetham, A.K., Ruhle, M., Kroto, H.W., and Walton, D.R.M., *Adv. Mater.*, 1999, vol. 11, p. 655.
18. Terrones, M., Terrones, H., Grobert, N., Hsu, W.K., Zhu, Y.Q., Hare, J.P., Kroto, H.W., Walton, D.R.M., Kohler-Redlich, Ph., Ruhle, M., Zhang, J.P., and Cheetham, A.K., *Appl. Phys. Lett.*, 1999, vol. 75, no. 25, p. 3932.
19. Grobert, N., Terrones, M., Trasobares, S., Kordatos, K., Terrones, H., Olivares, J., Zhang, J.P., Redlich, Ph., Hsu, W.K., Reeves, C.I, Wallis, D.I., Zhu, Y.Q., Hare, J.P., Pidduck, A.J., Kroto, H.W., and Walton, D.R.M, *Appl. Phys. A: Mater. Sci. Process.*, 2000, vol. 70, p. 175.
20. Terrones, M., Grobert, N., Olivares, J., Zhang, J.P., Terrones, H., Kordatos, K., Hsu, W.K., Hare, J.P., Tomnsend, P.D., Prassides, K., Cheetham, A.K., Kroto, H.W., and Walton, D.R.M., *Nature*, 1997, vol. 388, no. 3, p. 52.
21. Tang, Ch., Golberg, D., Bando, Y., Xu, F.F., and Liu, B., *Chem. Commun.*, 2003, p. 3050.
22. Yudasaka, M., Kikuchi, R., Ohki, Y., and Yoshimuda, S., *Carbon*, 1997, vol. 35, no. 2, p. 195.
23. Deepak, F.L., John Neena Susan, Govindaraj, A., Kulkarni, G.U., and Rao, C.N.R., *Chem. Phys. Lett.*, 2005, vol. 411, nos. 4–6, p. 468.
24. Dai, H., Rinzler, A.G., Nikolaev, P., Thess, A., Colbert, D.T., and Smalley, R.E., *Chem. Phys. Lett.*, 1996, vol. 260, p. 471.
25. Kurt, R., Klinke, C., Bonard, J.-M., Kern, K., and Karimi, A., *Carbon*, 2001, vol. 39, no. 14, p. 2163.
26. Kurt, R. and Karimi, A., *Thin Solid Films*, 2000, vols. 377–378, p. 163.
27. Reshetenko, T.V., Avdeeva, L.A., Ismagilov, Z.R., Chuvilin, A.L., and Ushakov, V.A., *Appl. Catal., A*, 2003, vol. 247, no. 1, p. 51.
28. Downs, W.B. and Baker, R.T.K., *Carbon*, 1991, vol. 29, no. 8, p. 1173.
29. Kruissink, E.S., van Reijen, L.L., and Ross, J.R.H., *J. Chem. Soc., Faraday Trans.*, 1981, vol. 77, no. 1, p. 649.
30. Avdeeva, L.B., Goncharova, O.V., Kochubey, D.I., Novgorodov, B.N., and Plyasova, L.M., *Appl. Catal., A*, 1995, vol. 126, p. 125.
31. Karnaukhov, A.P., Fenelonov, V.B., and Gavrilov, V.Yu., *Pure Appl. Chem.*, 1989, vol. 61, no. 11, p. 1913.
32. Gregg, C.J. and Sing, K.S.W., *Adsorption, Surface Area and Porosity*, London: Academic, 1982.
33. *XPSPEAK 4.1 for Windows 95/98*, http://www.phy.cuhk.edu.hk/~surface/XPSPEAK/.
34. *Using XPS PEAK Version 4.1 (November 2000)*, http://sun.phy.cuhk.edu.hk/~surfase/XPSPEAK/XPSPEAKusersguide.doc.
35. Fenelonov, V.B., *Poristyi uglerod* (Porous Carbon), Novosibirsk: Inst. Kataliza, 1995.
36. Bernardo, C.A., Alstrup, I., and Rostrup-Nielson, J.R., *J. Catal.*, 1985, vol. 96, no. 2, p. 517.
37. Tavares, M.T., Bernardo, C.A., Alstrup, I., and Rostrup-Nielson, J.R., *J. Catal.*, 1986, vol. 100, no. 2, p. 545.
38. Fenelonov, V.B., Avdeeva, L.B., Goncharova, O.V., Okkel, L.G., Simonov, P.A., Derevyankin, A.Yu., and Likholobov, V.A., in *Preparation of Catalysts VI*, Poncelet, G., Ed., Amsterdam: Elsevier, 1995, p. 825.
39. Avdeeva, L.B., Goncharova, O.V., Kochubey, D.I., Zaikovskii, V.I., Plyasova, L.M., Novgorodov, B.N., and Shaikhutdinov, Sh.K., *Appl. Catal.*, 1996, vol. 141, nos. 1–2, p. 117.
40. Buyanov, R.A., *Zakoksovanie katalizatorov* (Catalyst Coking), Novosibirsk: Nauka, 1983.
41. Alstrup, I., *J. Catal.*, 1988, vol. 109, no. 2, p. 241.
42. Rostrup-Nielson, J.R., *J. Catal.*, 1984, vol. 85, no. 1, p. 31.
43. Nishiyama, Y. and Tamai, Y., *J. Catal.*, 1976, vol. 45, no. 1, p. 1.
44. Mishakov, I.V., Chesnokov, V.V., Buyanov, R.A., and Chuvilin, A.L., *Dokl. Akad. Nauk*, 2002, vol. 386, no. 1, p. 65 [*Doklady Phys. Chem.* (Engl. Transl.), vol. 386, nos. 1–3, p. 207].

45. Jansen, R.J. and Bekkum, H.V., *Carbon*, 1995, vol. 33, no. 8, p. 1021.
46. Schmiers, H., Friebel, J., Streubel, P., Hesse, R., and Kopsel, R., *Carbon*, 1999, vol. 37, no. 12, p. 1965.
47. Yudasaka, M., Kikuchi, R., Ohki, Y., and Yoshimuda, S., *Carbon*, 1997, vol. 35, no. 2, p. 195.
48. Moulder, J.F., Stickle, W.F., Sobol, P.E., and Bomben, K.D., *Handbook of X-ray Photoelectron Spectroscopy*, Chastain, J., Ed., Eden Prairie, MN: Perkin-Elmer, 1992.
49. Stanczyk, K., Dziembal, R., Piwowarska, Z., and Witkowski, S., *Carbon*, 1995, vol. 33, no. 10, p. 1383.
50. Jian, M., Rico, CerdaJ.L., and Prins, R., *Bull. Soc. Chim. Belg.*, 1995, vol. 104, nos. 4–5, p. 225.
51. Chu Yongium, Wei Zhaobin, Yang Shuwn, Li Can, Xin Qin, and Min Enze., *Appl. Catal., A*, 1999, vol. 176, no. 1, p. 17.
52. Sonnemas, J., Neyens, W.J., and Mars, P., *J. Catal.*, 1974, vol. 34, no. 2, p. 230.
53. Hadjiloizou, G.C., Butt, J.B., and Dranoff, J.C., *J. Catal.*, 1991, vol. 131, no. 2, p. 545.